

Communication

# Suppression of the Equivalent Magnetic Noise Caused by Electron Spin Polarization in a Xe Isotope Comagnetometer

Zekun Wu <sup>1,2,\*</sup>, Zhen Chai <sup>1,2,\*</sup> , Lan Xiao <sup>1,2</sup> and Zhanchao Liu <sup>1,2,\*</sup><sup>1</sup> School of Instrumentation and Optoelectronic Engineering, Beihang University, Beijing 100191, China<sup>2</sup> Hefei National Laboratory, Hefei 230088, China

\* Correspondence: zhenchai@buaa.edu.cn (Z.C.); liuzc@buaa.edu.cn (Z.L.)

**Abstract:** The Xe isotope comagnetometer in the nuclear magnetic resonance regime can be used as a promising high-precision inertial measurement unit because of the absolute frequency measurement and high bandwidth. The fluctuation of the electron spin polarization leads to equivalent magnetic noise in the Xe isotope comagnetometer, which is one of the main factors limiting the stability of the comagnetometer. Here, we demonstrate systematic research of equivalent magnetic noise suppression and analyze the influence of the electron spin polarization on the Xe isotope comagnetometer. Based on the spin-exchange method between Xe isotopes and alkali metal atoms through the Fermi contact hyperfine interaction, the error equation of the Xe Larmor frequency is established. The equivalent magnetic noise can be suppressed by controlling the static magnetic field. This suppression method for Xe isotope comagnetometers improved the stability while maintaining high bandwidth. The experimental results show that this method can reduce the fluctuations of the <sup>129</sup>Xe and <sup>131</sup>Xe frequencies by 75% and 68.6%, respectively.

**Keywords:** Xe isotope comagnetometer; electron spin polarization; noise suppression; equivalent magnetic noise



**Citation:** Wu, Z.; Chai, Z.; Xiao, L.; Liu, Z. Suppression of the Equivalent Magnetic Noise Caused by Electron Spin Polarization in a Xe Isotope Comagnetometer. *Photonics* **2023**, *10*, 423. <https://doi.org/10.3390/photonics10040423>

Received: 14 February 2023

Revised: 2 April 2023

Accepted: 4 April 2023

Published: 9 April 2023



**Copyright:** © 2023 by the authors. Licensee MDPI, Basel, Switzerland. This article is an open access article distributed under the terms and conditions of the Creative Commons Attribution (CC BY) license (<https://creativecommons.org/licenses/by/4.0/>).

## 1. Introduction

Atomic comagnetometers using optically pumped alkali metal atoms to polarize noble gas molecules have a great advantage of having the long coherence time of the nuclear spin [1–3]. Benefiting from the absolute frequency measurement and high bandwidth, comagnetometers in the nuclear magnetic resonance (NMR) regime are widely used in searching for axion-like dark matter [4–6] and the inertial measurement [7,8]. Moreover, the system of Xe isotopes mixed with alkali metal atoms is a universal choice to suppress the effects of the ambient stray field [9–11]. The collisions of the Xe isotopes with polarized alkali metal atoms result in an effective magnetic field proportional to the electron spin polarization, which can shift the Xe Larmor frequency [12,13]. Therefore, the equivalent magnetic noise caused by the fluctuation of the electron spin polarization is undesired for the stability of the Xe isotope comagnetometer.

The electron spin polarization is mainly affected by the temperature, intensity, and frequency of the pump beam [14,15]. Many researchers suppressed the equivalent magnetic noise by only controlling a single factor, such as the stability of the pump beam frequency based on the light absorption method [16,17], the stability of the pump beam intensity relying on additional instruments [15,18], and the optimal temperature [19–21]. They lacked an overall analysis of the equivalent magnetic noise and failed to consider the electron spin polarization as a whole.

In this study, we demonstrate systematic research of equivalent magnetic noise suppression, and study the influence of the electron spin polarization on the Xe isotope comagnetometer operated in the NMR regime. We describe the spin exchange between Xe isotopes and alkali metal atoms through the Fermi contact hyperfine interaction, and

then obtain the error equation of the Xe Larmor frequency. The absolute electron spin polarization in different average photon spins is measured based on the free induction decay (FID) method to assess the magnitude of the equivalent magnetic noise. By analyzing the factors affecting the Xe Larmor frequency, we found that the equivalent magnetic noise can be suppressed by controlling the static magnetic field. The long-term stability of the Xe isotope comagnetometer is measured in the open-loop control and closed-loop control. Additionally, the impact of this method on the bandwidth is experimentally studied.

## 2. Principle

In the vapor cell of a Xe isotope comagnetometer, the nuclear spins are polarized by the spin–exchange interaction with alkali metal atoms that are optically pumped by the circularly polarized light. Neglecting the interaction between the neighboring nuclei, the dynamics of the comagnetometer with nuclear magnetization  $\mathbf{K}$  can be described using the Bloch equation as [22]:

$$\frac{d\mathbf{K}}{dt} = -\omega \times \mathbf{K} - \{\Gamma_2^n, \Gamma_2^n, \Gamma_1^n\} \cdot \mathbf{K} + \mathbf{R}_{se} \quad (1)$$

where  $\omega = \gamma_n \mathbf{B}$  is the effective Larmor frequency of the nuclear spins related to the applied magnetic field, the effective magnetic field  $B_e$ , and the inertial rotation  $\omega_R$ .  $\gamma_n$  is the gyromagnetic ratio. The separate matrix term accounts for the longitudinal relaxation rate  $\Gamma_1^n$  and transverse relaxation rate  $\Gamma_2^n$ . Additionally,  $\mathbf{R}_{se}$  is determined by the spin–exchange interaction between noble gas molecules and polarized alkali metal atoms. The effective magnetic field of the alkali metal atoms due to the Fermi contact interaction can be expressed as [23,24]:

$$B_e = -\kappa \frac{8\pi g_s \mu_B}{3} n_e P_e \quad (2)$$

where  $g_s \approx 2$ ,  $\mu_B$  is the electron magnetic moments.  $n_e$  is the density of the alkali metal atoms.  $\kappa$  is the enhancement factor for the Rb–Xe ensemble, which varies in amplitude for the Xe isotopes [13]. The electron spin polarization  $P_e$  can be expressed as [25]:

$$P_e = s \frac{R_{op}}{R_{op} + R_{rel}} \quad (3)$$

where the alkali metal atoms are polarized by the pump beam at the pump rate  $R_{op}$  and the average photon spin  $s$ . The alkali relaxation rate  $R_{rel}$  exists due to the volume of the cell and the motion of atoms and molecules [26,27]. The optical pumping rate is related to the intensity and frequency of the pumping beam fitting Voigt profiles, which can be expressed as [27]:

$$R_{op} = \frac{I_0}{h\nu r^2} r_e c f \sum_{F,F'} A_{F,F'} \text{Re}[V(\mathbf{v}_s \cdot \mathbf{v}_{F,F'})] \quad (4)$$

where  $I_0$  is the pumping intensity and  $r$  is the spot radius,  $h$  is the Plank constant and  $\nu$  is the frequency of the pumping beam,  $r_e$  is the classical electron radius,  $c$  is the light velocity,  $f$  is the oscillator strength, and  $A_{F,F'}$  is the transition strength. In this case, the drift of the pumping beam intensity and frequency will cause instability for the electron spin polarization, which can cause the equivalent magnetic noise  $\delta B_e$ . According to Equation (3), the electron spin polarization changes linearly with the average photon spin. When alkali metal atoms are pumped by the light of the ellipticity  $\frac{\pi}{4} - \alpha$ , the average photon spin  $s$  is provided by  $s = \cos 2\alpha$  [25,28] (define that  $\alpha$  is the angle of the fast axis of the quarter-wave plate with respect to the polarization axis of the polarized beam splitter). It is possible to suppress the equivalent magnetic noise by controlling the ellipticity of the pumping beam, but this will adversely affect the spin–exchange rate  $\mathbf{R}_{se}$ .

The Larmor frequency of Xe isotopes with the equivalent magnetic noise can be expressed as:

$$\omega_a = \gamma_a (B_0 + B_e^a + \delta B_e^a) + \omega_R \quad (5)$$

$$\omega_b = -\gamma_b (B_0 + B_e^b + \delta B_e^b) - \omega_R \tag{6}$$

where  $B_0$  is the static magnetic field applied along the pump beam. The subscript or superscript  $a$  and  $b$  correspond to  $^{129}\text{Xe}$  and  $^{131}\text{Xe}$ , respectively. Besides that, the Xe isotopes respond oppositely to the inertial rotation since their nuclear spins have opposite signs. The inertial rotation can be eliminated by adding the Larmor frequencies of the Xe isotopes, which can be expressed as:

$$\omega_{sum} = (\gamma_a - \gamma_b)B_0 + \gamma_a B_e^a \left(1 - \frac{\gamma_b}{\gamma_a} \Delta B_e\right) \tag{7}$$

where  $\Delta B_e$  is the equivalent magnetic noise. The high-order noise can be omitted, which is far less than the equivalent magnetic field. Alternatively, the static magnetic field  $B_0$  can be controlled to suppress the equivalent magnetic noise. In this way, when the Larmor frequencies of the Xe isotopes are summarized, the sum frequency only corresponds to the magnetic field and is unaffected by the inertial rotation. It can be seen from Equation (7) that the sum frequency contains two parts: the static magnetic field part and the equivalent magnetic noise part. Both changing  $B_0$  and  $\delta B_e$  can adjust the magnetic field along the  $z$ -axis to change the precession frequency of the Xe isotopes. Therefore, by controlling  $B_0$  to compensate  $\delta B_e$ , the sum frequency can keep the stability. We designed a closed-loop control of the static magnetic field to suppress the influence of the equivalent magnetic noise on the precession frequency stability for both  $^{129}\text{Xe}$  and  $^{131}\text{Xe}$ .

### 3. Experimental Setup

Figure 1 provides the schematic of a Xe isotope comagnetometer. The vapor cell with a 3 mm inner-side length is heated to 120 °C by two homemade polyimide heaters, filled with 5 Torr  $^{129}\text{Xe}$ , 20 Torr  $^{131}\text{Xe}$ , 20 Torr  $\text{N}_2$ , 200 Torr  $^4\text{He}$ , and a small drop of Rb. A three-dimensional Helmholtz coil designed in our system produces uniform magnetic fields and compensates for the residual magnetism. The static magnetic field along the  $z$ -axis is generated using an ultra-low noise current source whose noise density is 4 nA/ $\sqrt{\text{Hz}}$  (Stanford Research Systems CS580). The magnetic shield is set up outside the coils to weaken the effect of an external magnetic field. The pump beam with the frequency at the Rb D1 line first passes through the lens to acquire a 2.5 mm diameter. By rotating the half-wave plate, the intensity of the pump beam after the polarized beam splitter is set to 2 mW and linear polarization is ensured. A quarter-wave plate establishes the pump beam at a circular polarization to optically pump the alkali metal atoms. By using a neutral density filter, the probe beam is adjusted to 1 mW. The pump and probe laser are both emitted by the same type of DBR laser diodes (Photodigm PH795DBR080TS) and are driven by the circuit produced by UniQuanta. Passing through the vapor cell, the probe beam is separated into two mutually perpendicular linearly polarized beams using a polarized beam splitter. The signal of the comagnetometer is obtained by a balanced photodetector (Thorlabs PDA015A) and is processed in a lock-in amplifier (Zurich Instruments HF2LI). The concrete operation process can be accomplished in PC software (LabOne), which is applied by Zurich Instruments. As a result of the demodulation and filtering of the original signal from the balanced photodetector, the real-time Larmor frequencies of Xe isotopes can be obtained. The nuclear response curves can be measured by sweeping the frequency of the oscillating magnetic field along the  $x$ -axis. The resonant frequency is the Larmor frequency of the Xe isotope. The sum frequency ( $\omega_a^{ref} + \omega_b^{ref}$ ) is regarded as the reference frequency. By comparing the real-time frequency and the reference frequency, the frequency discriminator calculates the difference between them and inputs it into the PID controller. It is necessary to ensure that the real-time output frequency of the nucleus is equal to the set value. The driving current consists of the output signal of the PID controller and the DC current input to the  $z$ -axis coil to control the static magnetic field.

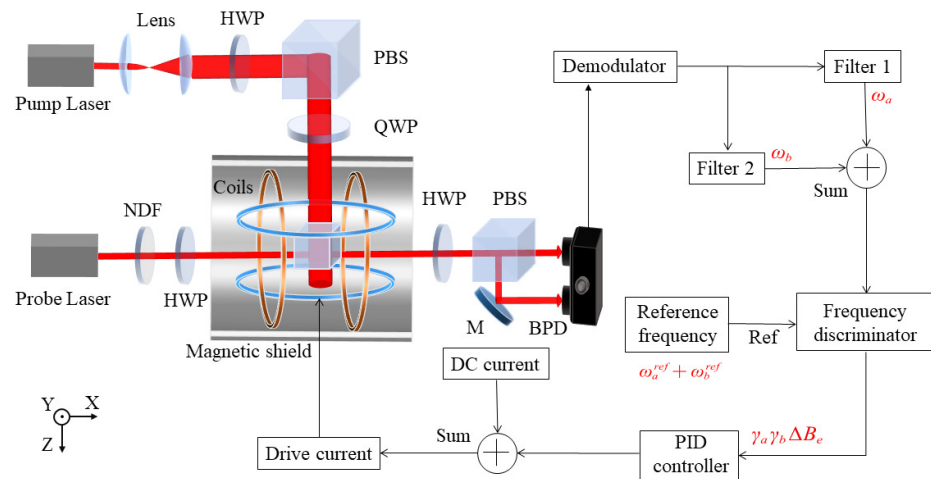


**Figure 1.** The schematic of a Xe isotope comagnetometer and processing. HWP: half-wave plate, QWP: quarter-wave plate, PBS: polarized beam splitter, PD: photodetector, NDF: neutral density filter, BPD: balanced photodetector, and Ref: reference signal used in the frequency discriminator.

#### 4. Results and Discussion

To assess the magnitude of the equivalent magnetic noise, the electron spin polarization is measured by the nuclear frequency shift  $\Delta\nu_n$ , which is widely used in the spin–exchange optical pumping system [14,15,29]. The equivalent magnetic field produced by electron spin polarization can be calculated by  $\Delta\nu_n = \gamma_n B_e$ . Firstly, the alkali metal atoms are pumped by a circularly polarized beam. A  $\pi/2$  pulsed magnetic field is applied along the  $x$ -axis to drive the  $^{129}\text{Xe}$  precession and the coherence decays naturally. Then, the pump beam is blocked before the next  $\pi/2$  pulsed magnetic field is applied. An example set for free induction decay (FID) signal and its Fast Fourier Transform (FFT) is shown in Figure 2. The black line is measured with the optical pump condition, and the red line is without the laser irradiation. The nuclear frequency shift is 0.191 Hz corresponding to a 16.1 nT equivalent magnetic field.

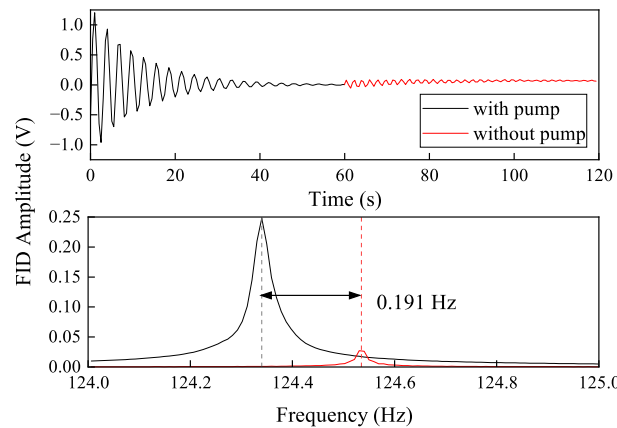


**Figure 2.** Top: FID signal of  $^{129}\text{Xe}$  with and without a circular pump beam. Bottom: FFT of transients.

The relationship between the electron spin polarization and the average photon spin can be obtained by rotating the QWP, while the other operations remain unchanged. We calculated the electronic spin polarization of the simulation results and compared it with the experiment as shown in Figure 3. The measured results are also based on the nuclear frequency shift method as described above. As the average photon spin changes from 1 to 0.18 (corresponding to  $\alpha$  from  $0^\circ$  to  $40^\circ$ ), the electronic spin polarization decreases gradually from 0.54 to 0.2. This indicates a change in the equivalent magnetic field of 5.96 nT. However, the signal-to-noise ratio of the comagnetometer will be affected by

changing the average photon spin. The low electron spin polarization is able to cause a false signal and influence the system sensitivity.

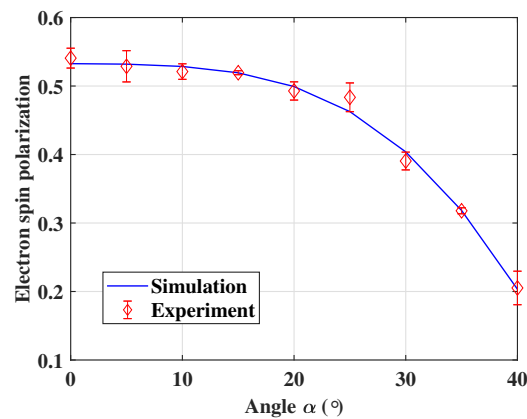


**Figure 3.** Comparison of the experimental results with simulations of the electron spin polarization in different ellipticity. The error bars represent the maximum and minimum values in the repeated experiments.

In the following, we study the suppression of the equivalent magnetic noise by controlling the static magnetic field. The reference frequency is acquired from the analysis of the frequency response for different magnitudes of the static magnetic field as shown in Figure 4. The magnetic linewidth is the transverse relaxation rate that consists of the relaxation in alkali metal collisions, the relaxation due to collisions with the cell wall surface, the relaxation due to magnetic-field inhomogeneities, and the gas-phase relaxation due to the self-collisions of the noble gas atoms [30,31]. Each of the blue, pink, green, and yellow dots and lines corresponds to the static magnetic field  $B_0$  at 10.79  $\mu\text{T}$ , 10.82  $\mu\text{T}$ , 10.85  $\mu\text{T}$ , and 10.88  $\mu\text{T}$ . Figure 4a shows that the Larmor precession frequency of  $^{129}\text{Xe}$  changes from 127.430 Hz to 128.483 Hz. Likewise, the Larmor precession frequency of  $^{131}\text{Xe}$  changes proportionally, as shown in Figure 4b. With the increasing magnitude of the static magnetic field, the Larmor frequency of Xe isotopes rises, which is consistent with Equations (5) and (6).

To further verify the linear relationship described in Equations (5) and (6), the Larmor frequencies of the Xe isotopes are measured at a series of static magnetic fields, as shown in Figure 5. The coefficient of determining the R-Square of the Xe isotopes' experimental data are both larger than 98.6%, which describes a good linearity of the static magnetic field and the Larmor frequency of the Xe isotopes. The inset figure represents the ratio of the two frequencies under different magnitudes of the static magnetic field. The ratio is a constant when the equivalent magnetic noises equal to zero. When the equivalent magnetic noise cannot be ignored, the ratio tends to maintain a steady level with the growing of  $B_0$ , thus indicating the synchronization and stability of the inertial information in the Xe isotope measurements.

The theoretical value marked in the solid line approximates the ratio of the spin magnetic ratios of the Xe isotopes. In addition, it is easier to control the static magnetic field than the average photon spin in the experimental operations. Therefore, controlling the static magnetic field is a better way to suppress the equivalent magnetic noise caused by electron spin polarization.

The real-time Larmor frequencies of Xe isotopes in the static magnetic field of open-loop control and closed-loop control are measured over 15 h, as shown in Figure 6. The open-loop control is conducted in the first 9 h, in which the range of frequency fluctuations of  $^{129}\text{Xe}$  and  $^{131}\text{Xe}$ , due to the equivalent magnetic noise, is 0.01 Hz and 0.0035 Hz, respectively. The closed-loop control conducted in the last 6 h is applied to suppress the long-term drift caused by this noise. The variation in the frequency fluctuations of  $^{129}\text{Xe}$  and  $^{131}\text{Xe}$  are 0.0025 Hz and 0.0011 Hz, respectively, reduced by 75% and 68.6%. This notably reduces

the interference of the noise and improves the stability of the Xe isotope comagnetometer. A greater enhancement of the noise suppression effect is restricted by magnetic field gradient produced by inhomogeneous electron spin polarization and errors introduced by signal processing. Figure 7 shows the signal noise measurement results of the Xe isotope comagnetometer under the same conditions of Figure 6. According to the experimental test results, the signal noise of the co-magnetometer in closed-loop control is lower than it in the open-loop control. Both frequencies of  $^{129}\text{Xe}$  and  $^{131}\text{Xe}$  have better performance under the closed-loop control. The noise level of  $^{129}\text{Xe}$  is greater than  $^{131}\text{Xe}$  because of the larger gyromagnetic ratio.

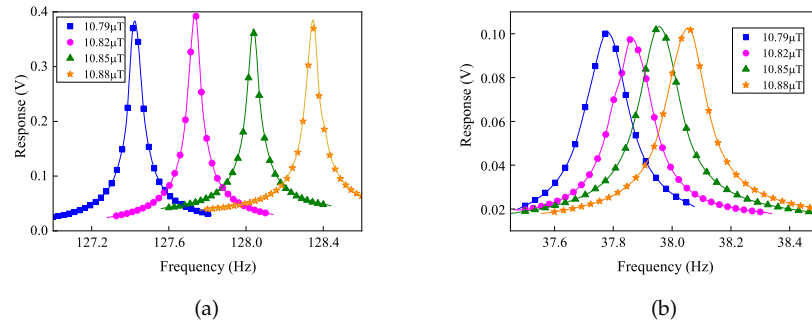


**Figure 4.** Xe isotopes response amplitudes (a)  $^{129}\text{Xe}$ , (b)  $^{131}\text{Xe}$  under different magnitudes of the static magnetic field.  $B_0$  changes from 10.79  $\mu\text{T}$  to 10.88  $\mu\text{T}$ .

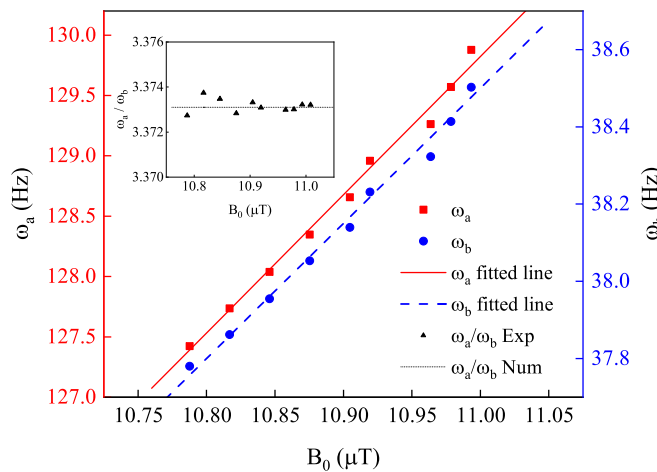


**Figure 5.** Measured nuclei Larmor frequency at different static magnetic fields. In the legend, the subscript “a” denotes  $^{129}\text{Xe}$ , and subscript “b” denotes  $^{131}\text{Xe}$ . Inset: dependence of the ratio of precession frequencies of  $^{129}\text{Xe}$  and  $^{131}\text{Xe}$ .

To assess the influence of this method on the bandwidth, the output frequency of the Xe isotope comagnetometer is measured as shown in Figure 8. As can be seen from Equations (5) and (6), the output frequency is provided by:

$$\omega_R = \frac{\gamma_a \omega_b + \gamma_b \omega_a}{\gamma_b - \gamma_a} \tag{8}$$

The input rotation rate changes from  $300^\circ/\text{s}$  to  $-300^\circ/\text{s}$  at a step of  $50^\circ/\text{s}$ , and Figure 8a shows the absolute frequency measured using the comagnetometer with the sampling rate at 200 Hz. The output frequencies calculated according to the standard that the method in each rotation rate (circle) are compared with the input signal (line), which can be seen in Figure 8b. The scale factor is 0.997. Thereby, our method to suppress the equivalent magnetic noise caused by electron spin polarization has realized a groundbreaking compromise between the stability and bandwidth.

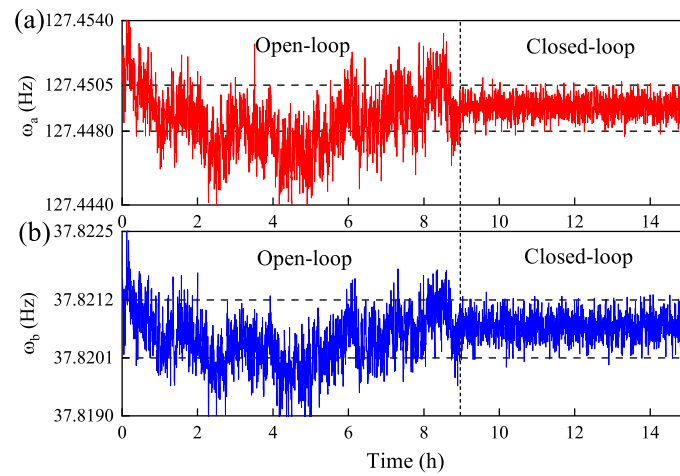


**Figure 6.** Experimental performance of the Xe isotopes under open-loop control and closed-loop control. (a) relates to  $^{129}\text{Xe}$ , while (b) relates to  $^{131}\text{Xe}$ . The frequencies of the Xe isotopes are measured simultaneously. The horizontal dashed lines indicate the noise level of the closed-loop control.

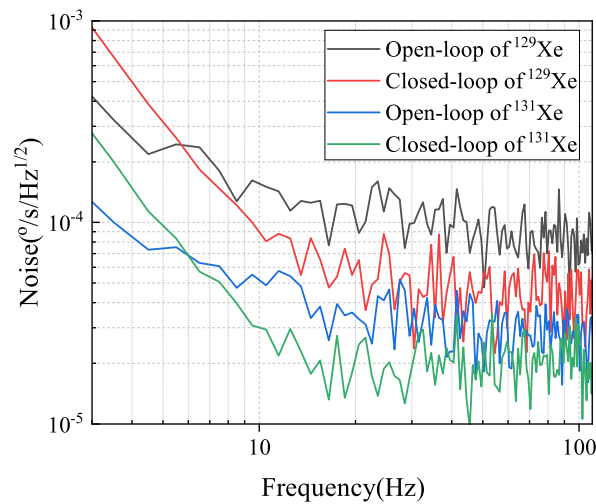


**Figure 7.** Comagnetometer signal noise of  $^{129}\text{Xe}$  and  $^{131}\text{Xe}$  under open-loop control and closed-loop control.

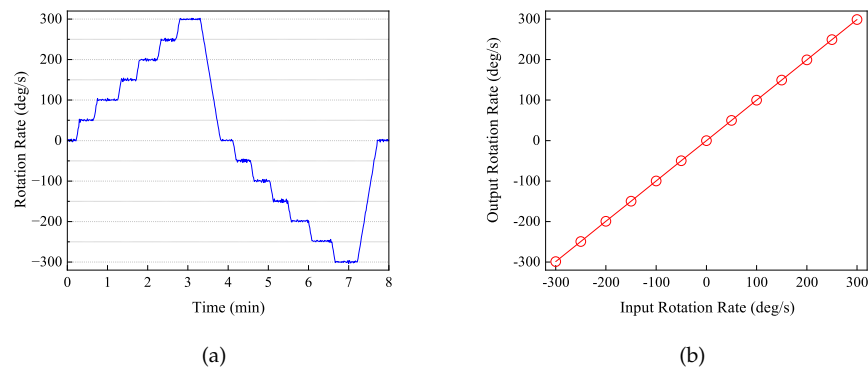


**Figure 8.** The output frequency  $\omega_R$  of the Xe isotope comagnetometer in rotation range from  $300^{\circ}/\text{s}$  to  $-300^{\circ}/\text{s}$ . (a) The output rotation rate in the time domain. (b) The relationship between input (line) and output (circle) rotation rate.

## 5. Conclusions

In conclusion, the influence of the electron spin polarization on the Larmor frequency of the Xe isotope comagnetometer was analyzed in this study. The drift of the pumping beam intensity and frequency causes fluctuation for the electron spin polarization, which can lead to the equivalent magnetic noise. We found that the equivalent magnetic noise can be suppressed by controlling the static magnetic field rather than adjusting the ellipticity of the pump beam, which can improve the stability while maintaining a high bandwidth. Experimentally, the long-term stability of the Xe isotope comagnetometer is measured under the open-loop and closed-loop operations. The fluctuations of the  $^{129}\text{Xe}$  and  $^{131}\text{Xe}$  frequencies have been reduced by 75% and 68.6%, respectively. This study provides a novel method to suppress the equivalent magnetic noise caused by electron spin polarization and has great significance in the performance of the Xe isotope comagnetometer.

**Author Contributions:** Conceptualization, Z.W. and Z.C.; methodology, Z.W.; software, Z.L.; validation, Z.W. and L.X.; formal analysis, Z.W.; investigation, Z.C.; resources, Z.C.; data curation, Z.W.; writing—original draft preparation, Z.W.; writing—review and editing, Z.C. and Z.L.; visualization, Z.W.; supervision, Z.L.; project administration, Z.L.; funding acquisition, Z.L. All authors have read and agreed to the published version of the manuscript.

**Funding:** This research was funded by Innovation Program for Quantum Science and Technology (2021ZD0300403) and National Science Fund for Distinguished Young Scholars (62225102).

**Institutional Review Board Statement:** Not applicable.

**Informed Consent Statement:** Not applicable.

**Data Availability Statement:** The data presented in this study are available from the corresponding author upon reasonable request.

**Conflicts of Interest:** The authors declare no conflict of interest.

## References

1. Meyer, D.; Larsen, M. Nuclear magnetic resonance gyro for inertial navigation. *Gyroscopy Navig.* **2014**, *5*, 75–82. [[CrossRef](#)]
2. Korver, A.; Thrasher, D.; Bulatowicz, M.; Walker, T. Synchronous spin-exchange optical pumping. *Phys. Rev. Lett.* **2015**, *115*, 253001. [[CrossRef](#)] [[PubMed](#)]
3. Walker, T.; Larsen, M. Spin-exchange-pumped nmr gyros. In *Advances in Atomic, Molecular, and Optical Physics*; Elsevier: Amsterdam, The Netherlands, 2016; pp. 373–401.
4. Afach, S.; Buchler, B.; Budker, D.; Dailey, C.; Derevianko, A.; Dumont, V.; Figueroa, N.; Gerhardt, I.; Grujic, Z.; Guo, H.; et al. Search for topological defect dark matter with a global network of optical magnetometers. *Nat. Phys.* **2021**, *17*, 1396–1401. [[CrossRef](#)] [[PubMed](#)]
5. Jiang, M.; Su, H.; Garcon, A.; Peng, X.; Budker, D. Search for axion-like dark matter with spin-based amplifiers. *Nat. Phys.* **2021**, *17*, 1402–1407. [[CrossRef](#)]
6. Jackson, D.; Afach, S.; Aybas, D.; Blanchard, J.; Budker, D.; Centers, G.; Engler, M.; Figueroa, N.; Garcon, A.; Graham, P.; et al. Overview of the cosmic axion spin precession experiment. In *Microwave Cavities and Detectors for Axion Research*; Springer: Berlin/Heidelberg, Germany, 2020; pp. 105–121.
7. Bevan, D.; Bulatowicz, M.; Clark, P.; Flicker, J.; Griffith, R.; Larsen, M.; Luengo-Kovac, M.; Pavell, J.; Rothballer, A.; Sakaida, D. Nuclear magnetic resonance gyroscope: Developing a primary rotation sensor. In Proceedings of the 2018 IEEE International Symposium on Inertial Sensors and Systems (INERTIAL), Lake Como, Italy, 26–29 March 2018; pp. 1–2.
8. Cipolletti, R.; Riedrich-Moeller, J.; Fuchs, T.; Wickenbrock, A.; Budker, D. Modeling of the transient behavior of a nuclear magnetic resonance gyroscope. In Proceedings of the 2021 IEEE Sensors, Sydney, Australia, 31 October–3 November 2021; pp. 1–4.
9. Hao, C.; Yuan, C.; Liu, S.; Sheng, D. Herriott-cavity-assisted closed-loop Xe isotope comagnetometer. *Phys. Rev. A* **2021**, *103*, 053523. [[CrossRef](#)]
10. Lee, S.; Yim, S.; Kim, T.; Kim, Z.; Shim, K. Lock-in-detection in  $^{87}\text{Rb}$ – $^{129}\text{Xe}$ / $^{131}\text{Xe}$  atom spin gyroscopes. *J. Phys. B-At. Mol. Opt. Phys.* **2020**, *53*, 035502. [[CrossRef](#)]
11. Zhang, K.; Zhao, N.; Wang, Y. Closed-loop nuclear magnetic resonance gyroscope based on Rb-Xe. *Sci. Rep.* **2020**, *10*, 1–7. [[CrossRef](#)]
12. Petrov, V.; Pazgalev, A.; Vershovskii, A. Isotope shift of nuclear magnetic resonances in  $^{129}\text{Xe}$  and  $^{131}\text{Xe}$  caused by spin-exchange pumping by alkali metal atoms. *IEEE Sens. J.* **2019**, *20*, 760–766. [[CrossRef](#)]

13. Bulatowicz, M.; Griffith, R.; Larsen, M.; Mirijanian, J.; Fu, C.; Smith, E.; Snow, W.; Yan, H.; Walker, T. Laboratory search for a long-range t-odd, p-odd interaction from axionlike particles using dual-species nuclear magnetic resonance with polarized  $^{129}\text{Xe}$  and  $^{131}\text{Xe}$  gas. *Phys. Rev. Lett.* **2013**, *111*, 102001. [[CrossRef](#)]
14. Liu, X.; Luo, H.; Qu, T.; Yang, K.; Ding, Z. Measuring the spin polarization of alkali-metal atoms using nuclear magnetic resonance frequency shifts of noble gases. *AIP Adv.* **2015**, *5*, 107119. [[CrossRef](#)]
15. Jia, Y.; Liu, Z.; Zhou, B.; Liang, X.; Wu, W.; Peng, J.; Ding, M.; Zhai, Y.; Fang, J. Pump beam influence on spin polarization homogeneity in the nuclear magnetic resonance gyroscope. *J. Phys. D-Appl. Phys.* **2019**, *52*, 355001.
16. Jia, Y.; Liu, Z.; Chai, Z.; Liang, X.; Wu, W. The optimization and stabilization of pump light frequency in the minimized atomic magnetometer. *IEEE Trans. Instrum. Meas.* **2021**, *70*, 1–9. [[CrossRef](#)]
17. Dudzik, G.; Rzepka, J.; Abramski, K. Polarization switching detection method using a ferroelectric liquid crystal for dichroic atomic vapor laser lock frequency stabilization techniques. *Appl. Opt.* **2015**, *54*, 2806–2813. [[CrossRef](#)] [[PubMed](#)]
18. Huang, J.; Fan, W.; Wang, Z.; Yuan, L.; Zhang, K.; Pei, H.; Pang, H.; Quan, H. Analysis and suppression of the misalignment error for the pumping laser in the atomic comagnetometer. *Opt. Express* **2022**, *30*, 6374–6387. [[CrossRef](#)]
19. Yin, Y.; Zhou, B.; Yin, K.; Wang, Y.; Tang, J.; Ye, M.; Ning, X.; Han, B. The influence of temperature and modulated magnetic field on the transmission intensity of atomic magnetometer. *J. Phys. D-Appl. Phys.* **2021**, *54*, 485001. [[CrossRef](#)]
20. Zhang, S.; Lu, J.; Ye, M.; Zhou, Y.; Yin, K.; Lu, F.; Yan, Y.; Zhai, Y. Optimal operating temperature of miniaturized optically pumped magnetometers. *IEEE Trans. Instrum. Meas.* **2022**, *71*, 1–7. [[CrossRef](#)]
21. Lee, W.; Lucivero, V.; Romalis, M.; Limes, M.; Foley, E.; Kornack, T. Heading errors in all-optical alkali-metal-vapor magnetometers in geomagnetic fields. *Phys. Rev. A* **2021**, *103*, 063103. [[CrossRef](#)]
22. Grebenkov, D. Nmr survey of reflected brownian motion. *Rev. Mod. Phys.* **2007**, *79*, 1077. [[CrossRef](#)]
23. Walker, T.; Happer, W. Spin-exchange optical pumping of noble-gas nuclei. *Rev. Mod. Phys.* **1997**, *69*, 629. [[CrossRef](#)]
24. Ma, Z.; Sorte, E.; Saam, B. Collisional  $^3\text{He}$  and  $^{129}\text{Xe}$  frequency shifts in Rb–noble-gas mixtures. *Phys. Rev. Lett.* **2011**, *106*, 193005. [[CrossRef](#)]
25. Seltzer, S. *Developments in Alkali-Metal Atomic Magnetometry*; Princeton University: Princeton, NJ, USA, 2008.
26. Happer, W.; Miron, E.; Schaefer, S.; Schreiber, D.; Van Wijngaarden, W.; Zeng, X. Polarization of the nuclear spins of noble-gas atoms by spin exchange with optically pumped alkali-metal atoms. *Phys. Rev. A* **1984**, *29*, 3092. [[CrossRef](#)]
27. Kornack, T. *A Test of CPT and Lorentz Symmetry Using a Potassium-Helium-3 Co-Magnetometer*; Princeton University: Princeton, NJ, USA, 2005.
28. Ding, Z.; Yuan, J.; Wang, Z.; Lu, G.; Luo, H. Optically pumped rubidium atomic magnetometer with elliptically polarized light. *Optik* **2016**, *127*, 5270–5273. [[CrossRef](#)]
29. Schaefer, S.; Cates, G.; Chien, T.; Gonatas, D.; Happer, W.; Walker, T. Frequency shifts of the magnetic-resonance spectrum of mixtures of nuclear spin-polarized noble gases and vapors of spin-polarized alkali-metal atoms. *Phys. Rev. A* **1989**, *39*, 5613. [[CrossRef](#)] [[PubMed](#)]
30. Yan, Y.; Lu, J.; Zhang, S.; Lu, F.; Yin, K.; Wang, K.; Zhou, B.; Liu, G. Three-axis closed-loop optically pumped magnetometer operated in the SERF regime. *Opt. Express* **2022**, *30*, 18300–18309. [[CrossRef](#)] [[PubMed](#)]
31. Liu, X.; Chen, C.; Qu, T.; Yang, K.; Luo, H. Transverse spin relaxation and diffusion-constant measurements of spin-polarized  $^{129}\text{Xe}$  nuclei in the presence of a magnetic field gradient. *Sci. Rep.* **2016**, *6*, 1–8. [[CrossRef](#)] [[PubMed](#)]

**Disclaimer/Publisher’s Note:** The statements, opinions and data contained in all publications are solely those of the individual author(s) and contributor(s) and not of MDPI and/or the editor(s). MDPI and/or the editor(s) disclaim responsibility for any injury to people or property resulting from any ideas, methods, instructions or products referred to in the content.